

# Precise Half-Life Measurement of the Superaligned $\beta^+$ Emitter $^{26}\text{Si}$

V.E. Iacob,\* J.C. Hardy, A. Banu,† L. Chen, V. V. Golovko,‡ J.  
Goodwin, V. Horvat, N. Nica,† H.I. Park, L. Trache, and R.E. Tribble  
*Cyclotron Institute at Texas A&M University*  
(Dated: August 18, 2010)

We have measured the half-life of the superallowed  $0^+ \rightarrow 0^+$   $\beta^+$  emitter  $^{26}\text{Si}$  to be 2245.3(7) ms. We used pure sources of  $^{26}\text{Si}$  and employed a high-efficiency gas counter, which was sensitive to positrons from both this nuclide and its daughter  $^{26}\text{Al}^m$ . The data were analyzed as a linked parent-daughter decay. To contribute meaningfully to any test of the unitarity of the Cabibbo-Kobayashi-Maskawa (CKM) matrix, the  $ft$  value of a superallowed transition must be determined to a precision of 0.1% or better. With a precision of 0.03% the present result is more than sufficient to be compatible with that requirement. Only the branching ratio now remains to be measured precisely before a  $\pm 0.1\%$   $ft$  value can be obtained for the superallowed transition from  $^{26}\text{Si}$ .

PACS numbers: 21.10.Tg, 23.40.-s, 27.30.+t

## I. INTRODUCTION

The unitarity of the Cabibbo-Kobayashi-Maskawa (CKM) matrix is a fundamental requirement of the three-generation Standard Model. Currently, the most demanding test available of CKM unitarity is the sum of squares of the experimentally determined elements of the matrix's top row [1]. The dominant term in this test is the up-down quark-mixing element,  $V_{ud}$ , the most precise value of which is obtained through nuclear measurements of superallowed  $0^+ \rightarrow 0^+$  beta decays. To date, the measured  $ft$  values for transitions from ten different nuclei are known to  $\sim 0.1\%$  precision and three more to  $\leq 0.3\%$  [1]. So far, the superallowed transition from  $^{26}\text{Si}$  has not been in either category, its  $ft$ -value precision being 0.8%, too large for it to contribute to the unitarity test.

Since a superallowed  $0^+ \rightarrow 0^+$  transition involves only the vector current, its  $ft$  value relates to the vector coupling constant,  $G_V$  – and, through it, to  $V_{ud}$  – via the relationship [1]

$$\mathcal{F}t \equiv ft(1 + \delta'_R)(1 + \delta_{NS} - \delta_C) = \frac{K}{2G_V^2(1 + \Delta_R^V)}, \quad (1)$$

where  $\mathcal{F}t$  is defined to be the “corrected”  $ft$  value and  $K/(\hbar c)^6 = 2\pi^3 \hbar \ln 2 / (m_e c^2)^5 = 8120.2787(11) \times 10^{-10} \text{ GeV}^{-4}\text{s}$ . There are four small correction terms:  $\delta_C$  is the isospin-symmetry-breaking correction;  $\Delta_R^V$  is the transition-independent part of the radiative correction; and the terms  $\delta'_R$  and  $\delta_{NS}$  comprise the transition-dependent part of the radiative correction, the former

being a function only of the maximum positron energy and the atomic number,  $Z$ , of the daughter nucleus, while the latter, like  $\delta_C$ , depends in its evaluation on the details of nuclear structure. Both  $\delta_C$  and  $\delta_{NS}$  have been calculated [2] with the best available shell-model wave functions, which are based on a wide range of spectroscopic data. They include those core orbitals that were determined to be important based on measured spectroscopic factors in single-nucleon pick-up reactions; and they were further tuned to agree with measured binding energies, charge radii and coefficients of the isobaric multiplet mass equation.

Although, in principle, the precise  $ft$  value for a single  $0^+ \rightarrow 0^+$  superallowed transition should be sufficient to determine  $V_{ud}$ , that would leave the validity of these structure-dependent corrections without independent verification, and the derived value for  $G_V$  could be in doubt. What has given credibility to the nuclear result for  $G_V$  is the fact that many superallowed transitions have been measured precisely and all give statistically identical results for  $\mathcal{F}t$  – and hence for  $G_V$ . Since the uncorrected  $ft$  values actually scatter over a relatively wide range, it is the structure-dependent corrections that are responsible for bringing the  $\mathcal{F}t$  values into agreement with one another.

Obviously, this is already a powerful experimental validation of the calculated corrections themselves, but it can be improved even further by precise measurements of additional transitions, especially ones calculated to have large correction terms. If the  $ft$  values measured for cases with large calculated corrections also turn into corrected  $\mathcal{F}t$  values that are consistent with the others, then this reinforces the calculations' reliability for cases in which the corrections are smaller. The calculated correction terms for the superallowed transition from  $^{26}\text{Si}$  give the result  $\delta_C - \delta_{NS} = 0.65(3)\%$  [2]. Although this value is not particularly large compared to most of the well-measured cases, it is more than double the size of the correction for the superallowed transition from  $^{26}\text{Al}^m$ , which is its mirror transition. Experimental verification of this pre-

\*iacob@comp.tamu.edu; On leave from the National Institute for Physics and Nuclear Engineering “Horia Hulubei”, Bucharest, Romania.

†On leave from the National Institute for Physics and Nuclear Engineering “Horia Hulubei”, Bucharest, Romania.

‡Present address: Department of Physics, Queen's University, Stirling Hall, Kingston, ON, K7L 3N6, Canada.

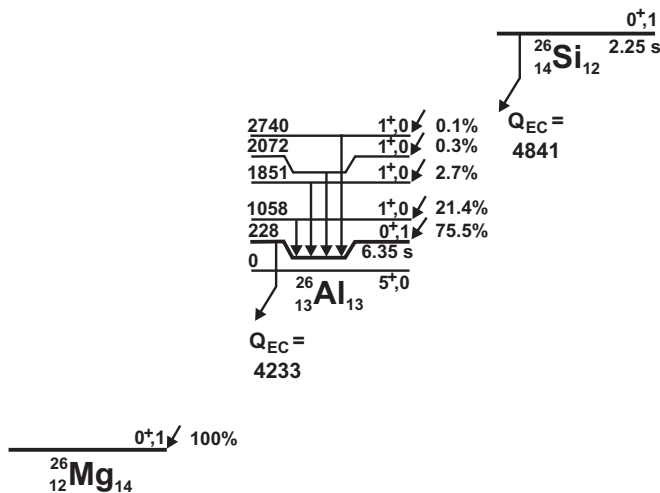


FIG. 1: Combined decay schemes of  $^{26}\text{Si}$  and  $^{26}\text{Al}^m$  showing only those features of relevance to their superallowed  $\beta$  decays. All energies are in keV and the  $Q_{EC}$  values shown are for the superallowed branch. The data are taken from Refs. [1, 6].

dicted mirror asymmetry would be a valuable test of the calculations.

The  $ft$  value that characterizes any  $\beta$ -transition depends on three measured quantities: the total transition energy,  $Q_{EC}$ , the half-life,  $t_{1/2}$ , of the parent state and the branching ratio,  $R$ , for the particular transition of interest. The  $Q_{EC}$ -value is required to determine the statistical rate function,  $f$ , while the half-life and branching ratio combine to yield the partial half-life,  $t$ . The  $Q_{EC}$  value for  $^{26}\text{Si}$  is already known sufficiently well [3] to yield a value for  $f$  with 0.015% precision but, before the measurement reported here, the  $^{26}\text{Si}$  half life was only known to 0.12% and its branching ratio to 0.8% [1]. Our new half-life for  $^{26}\text{Si}$  has 0.03% precision and furthermore disagrees significantly with the measurement [4] that previously dominated the world average. The result reported here represents our first step in bringing the precision of the  $ft$  value for this transition into the desired range of 0.1%. The second step will be an improved branching ratio, a measurement that we will soon undertake.

Like the decay of  $^{34}\text{Ar}$ , whose half-life we have reported previously [5],  $^{26}\text{Si}$   $\beta^+$  decays to a daughter which is itself radioactive and is, in fact, another superallowed emitter. The combined decay schemes appear in Fig. 1, where it can be seen that the half-life of  $^{26}\text{Al}^m$ , the daughter, differs by only a factor of three from that of  $^{26}\text{Si}$ . This adds complications to the experiment, which requires us to use the techniques that we developed previously for our study of  $^{34}\text{Ar}$ . These will be described briefly in the following sections, but for further details the reader is referred to Ref. [5].

## II. EXPERIMENT

### A. Overview

Precise half-life measurements need high-purity radioactive beams, a requirement that is even more important for cases where the daughter nucleus is also radioactive with a similar half-life. We achieved this goal by using a production reaction with inverse kinematics,  $p(^{27}\text{Al}, 2n)^{26}\text{Si}$ , and selecting the desired reaction product with the Momentum Achromat Recoil Separator (MARS) [7]. Our primary beam of 30.4-MeV  $^{27}\text{Al}$ , which was produced by the superconducting cyclotron at Texas A&M University, impinged on a 1.6-atm hydrogen gas target cooled to liquid nitrogen temperature. The fully stripped ejectiles were then analyzed by MARS. Initially, working with a low-current primary beam, we inserted at the focal plane of MARS a  $5 \times 5$  cm silicon telescope consisting of a 16-strip position-sensitive detector (PSD) 300  $\mu\text{m}$  thick, backed by a 1-mm-thick detector. The telescope was used first for the identification of secondary reaction products, then for the control of the selection and focus of the desired species in the center of the beam line. This also gave us a clear indication of nearby reaction products that could potentially contribute as impurities to our selected beam.

After the tuning and selection procedure, the PSD was dropped out of the way and the intensity of the primary beam was increased. With extraction slits at the MARS focal plane used to select  $^{26}\text{Si}$ , the resulting 25.2-A-MeV radioactive beam was extracted into air through a 51- $\mu\text{m}$ -thick kapton window. This beam, typically of  $2 \times 10^4$  ions per second, passed through a 0.3-mm thin BC-404 plastic scintillator, where the ions were counted, and then through a set of aluminum degraders, eventually being implanted in the 76- $\mu\text{m}$ -thick aluminized mylar tape of a fast tape-transport system. The combination of  $m/q$  selectivity in MARS and range selectivity in the degraders led to implanted samples that were at least 99.8% pure.

After the radioactive sample had been collected for a time interval of the order of the  $^{26}\text{Si}$  half-life, the beam was turned off and the tape-transport system moved the sample in  $\sim 175$  ms to a well-shielded location 90 cm away, stopping it in the center of a  $4\pi$  proportional gas counter. The decay positrons were then detected for twenty half-lives (45 s), with signals from the gas counter being multiscaled into a 500-channel time spectrum. These collect-move-detect cycles were computer controlled and their timing was continuously monitored on-line. They were repeated, with a separate decay spectrum recorded for each, until the desired overall statistics had been achieved. In its shielded location, the gas counter had a background rate of about 0.5 counts/s, which was 3-4 orders of magnitude lower than the initial count rate for each collected sample. For this experiment we accumulated data from 5,000 cycles split into 55 separate runs, which yielded a total of  $2 \times 10^8$  counts.

## B. Gas counter and electronics

The gas counter we used is similar to ones we have used in previous precise half-life measurements [5, 8–11]. It consists of two separate gas cells that, when assembled, have a 0.25-mm slot between them, through which the mylar transport-tape passes. Both cells were machined from copper and each is equipped with anodes of 13- $\mu$ m-diameter gold-plated tungsten wire. Methane at just over one-atmosphere pressure is continuously flushed through both cells. Methane offers adequate gas gain for detecting positrons and is quite insensitive to  $\gamma$  radiation. A Havar foil window, 3.7 cm in diameter and 1.5  $\mu$ m thick, hermetically seals each gas cell on the side facing the tape.

The electronic chain we used in the measurement was the same as that described in detail in Ref. [5]. The pre-amplified signal from the gas counter is first passed to a fast-filter amplifier with high gain ( $\times 500$ ). At this high gain many of the pulses would saturate the amplifier so, to ensure that the amplifier recovers quickly, large pulses are clipped with a Schottky diode inserted after its first stage of amplification. The amplified and clipped pulses are then passed to a discriminator with very low threshold (150–250 mV).

A  $^{90}\text{Sr}/^{90}\text{Y}$   $\beta$  source is used to set up the detector system. This source has been specially prepared on a sample length of transport tape and is inserted into the gas counter in exactly the position that an on-line sample, such as  $^{26}\text{Si}$ , is situated. Our procedure is to record, at a fixed threshold setting, the counting rate from the discriminator as a function of the applied counter bias voltage. Initially, as the applied voltage is raised the count-rate also rises since the increasing gas gain leads to more primary ionizing  $\beta$  events triggering the discriminator. However, at approximately 2600 volts – the exact value depends on the threshold setting – a “plateau” is reached, and the count rate remains nearly unchanged for the next 200–300 volts increase in the bias voltage. At higher voltages still, there is a second rapid rise in the count rate as spurious pulses increasingly trigger the discriminator. This behavior is well understood [12] and clearly demonstrates that, when operated in the plateau region, such detectors have essentially 100% efficiency. During our  $^{26}\text{Si}$  measurement the detector was always operated in the plateau region.

Since dead-time is a serious concern for half-life measurements, the discriminator output signals were split and sent to two fixed-width, non-retriggering and non-extending gate generators, which established different dominant dead times in the two separate streams, both of which were multiscaled. The time base for the multiscalers was defined by a function generator, which is accurate to 0.01 ppm. Both gates also were continuously monitored during every run, thus giving us an on-line measure of the dead-time ( $\pm 5$  ns) during data collection. Note that even though the two gate generators were fed by the same data, the dead-time distortions of the un-

derlying Poisson-distributed data are independent in the two cases; thus the two data streams allowed us to test that our dead-time corrected result was independent of the actual dead time of the circuit.

## C. Special precautions

As the experiment was aimed at better than 0.1% precision, many tests for systematic effects were made and special precautions taken during the measurements themselves:

- Every experiment was subdivided into many separate runs, differing only in their particular combination of detection parameters: dominant dead-time, detector bias and discrimination threshold. We used combinations of four different dead times (3, 4, 6 and 8  $\mu$ s), three discriminator thresholds (150, 200 and 250 mV) and four detector biases (2550, 2650, 2750 and 2850 V). The separate analysis of each individual run allowed us to test for systematic effects that could contribute to the uncertainty in the final result.
- Since each  $^{26}\text{Si}$  decay produces an  $^{26}\text{Al}^m$  daughter that also decays, the relative activity of the two nuclides at the beginning of the detection period depends on the length of the collection period (and the tape-move time) that preceded it. We used four different collection times (1.0, 2.5, 3.0 and 4.5 s) to test for consistency.
- The ratio of the parent to daughter activities also depends on the time-dependence of the rate at which  $^{26}\text{Si}$  was accumulated in the tape during the collection period. The number of ions registered in the scintillator located just in front of the aluminum degraders was recorded as a function of time with each cycle, and the results were used in our analysis.
- The few weak impurities in the  $^{26}\text{Si}$  beam have different ranges in our degraders. Thus, any contribution they might make to the total activity collected in the tape would depend on the depth at which the  $^{26}\text{Si}$  beam is stopped in the tape. By using two different thicknesses of aluminum degrader we placed the  $^{26}\text{Si}$  midway through the 76- $\mu$ m tape for the first 30 runs and then near the rear surface for the remaining 25. Again we tested for consistent results.
- The tape-transport system is quite consistent in placing the collected source within  $\pm 3$  mm of the center of the detector, but it is a mechanical device, and occasionally larger deviations occur. We separately recorded the number of implanted nuclei detected in the scintillator during the collection period of each cycle, and the number of positrons

recorded in the gas counter during the subsequent count period. The ratio of the latter to the former is a sensitive measure of whether the source was seriously misplaced in the proportional counter.

- We checked the composition of the beam exiting MARS once per day by re-inserting the PSD and ensuring that no changes had occurred.
- Several background measurements were made, in which all conditions were identical to those of a normal run except that the tape motion was disabled.
- In one run, we repeatedly collected activity for 16.5 s and counted for 165 s in order to search for long-lived impurities. None was found.
- It is important that the gas counter be operated in the “plateau” region: *i.e.* within the range of detector bias voltages in which the counting rate is nearly independent of voltage at a given discriminator setting. We measured this voltage plateau with a long-lived  $^{90}\text{Sr}/^{90}\text{Y}$  source before and after our measurement, and once during it. In all cases we found the plateau slope to be  $\leq 0.5\%$  per 100 V and did not observe any changes in the voltage boundaries of the plateau region.

### III. ANALYSIS AND RESULTS

Before analyzing the data, we first removed any cycles that had fewer than 500 implanted  $^{26}\text{Si}$  ions detected by the scintillator. These were the result of low – or no – primary beam current from the cyclotron during part or all of the collection period. Then we eliminated those cycles with an anomalously low ratio of recorded positrons to implanted silicon ions, which is indicative of faulty tape motion leading to a misplaced sample in the gas detector. Approximately 8% of the cycles were rejected for this reason.

#### A. Parent-daughter connection

For each run, we processed the accepted data by summing the dead-time-corrected spectra from all its included cycles. We corrected for dead time using the procedure outlined in Ref. [9]. The total time-decay spectrum obtained from the combined runs is presented in Fig. 2, where we also show the separate contributions from the  $^{26}\text{Si}$  parent and  $^{26}\text{Al}^m$  daughter. This breakdown into components is based upon our final analysis and is presented here simply to illustrate how the parent-daughter decay curve, which combines two rather similar half-lives, tends to mask the parent half-life even though the parent activity dominates at the start of the counting period.

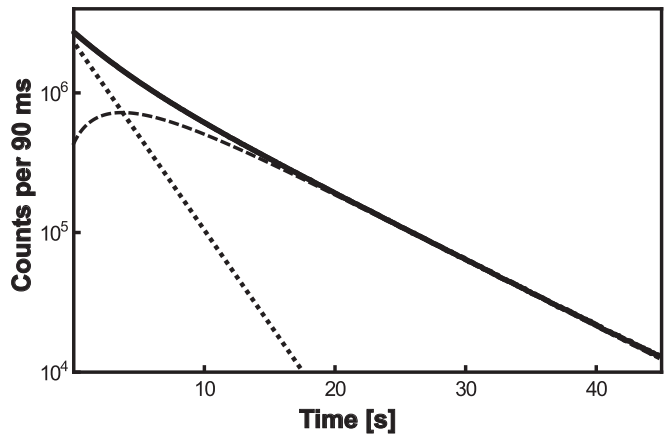


FIG. 2: Measured time-decay spectrum (solid line) for the total of all data obtained from the  $\beta^+$  decay of  $^{26}\text{Si}$  and its daughter  $^{26}\text{Al}^m$ . The dotted/dashed lines represent the derived  $^{26}\text{Si}/^{26}\text{Al}^m$  contributions.

We can easily understand this situation by examining the coupled decay equations for combined parent-daughter decays. The combined  $^{26}\text{Si}$  and  $^{26}\text{Al}^m$  activity yields a total rate for detected positrons of

$$\Lambda_{tot} = C_1 e^{-\lambda_1 t} + C_2 e^{-\lambda_2 t}, \quad (2)$$

with

$$\begin{aligned} C_1 &= N_1 \epsilon_2 \lambda_1 \left( \frac{\epsilon_1}{\epsilon_2} - \frac{\lambda_2}{\lambda_1 - \lambda_2} \right) \\ C_2 &= N_1 \epsilon_2 \lambda_2 \left( \frac{N_2}{N_1} + \frac{\lambda_1}{\lambda_1 - \lambda_2} \right), \end{aligned} \quad (3)$$

where  $t$  is the time elapsed after the end of the collect period;  $N_{1,2}$  are the numbers of  $^{26}\text{Si}$  and  $^{26}\text{Al}^m$  nuclei present in the sample at  $t = 0$ ;  $\epsilon_{1,2}$  are the experimental efficiencies for detecting the positrons from the respective decays; and  $\lambda_{1,2}$  are the corresponding decay constants. Note that when  $\lambda_1 = 2\lambda_2$  (and  $\epsilon_1 = \epsilon_2$ ) the coefficient  $C_1$  vanishes, leaving a single exponential term having the decay constant of the daughter. The half-lives of  $^{26}\text{Si}$  and  $^{26}\text{Al}^m$  are actually related by a factor of 2.8, close enough to 2 that, for our measurements, the coefficient  $C_1$  was slightly smaller than  $C_2$ , leaving the daughter to dominate the decay curve (see Fig. 2). This imposes a real limitation on the precision that can be obtained from a conventional fit to the data: even with  $\lambda_2$  fixed at its known value,  $C_1$ ,  $C_2$  and  $\lambda_1$  (as well as the constant background) must all be determined independently, which leads to  $\lambda_1$  having a rather large uncertainty.

We can overcome this limitation by fixing the ratio  $C_2/C_1$  so as to reduce the number of adjustable parameters in the fit to three (including background), as we did for our measurement of the  $^{34}\text{Ar}$  half-life [5]. In practice this means that we must establish two ratios,  $N_2/N_1$  and  $\epsilon_1/\epsilon_2$ , from the experimental parameters. In this section we deal with the former; in the next section, with the latter.

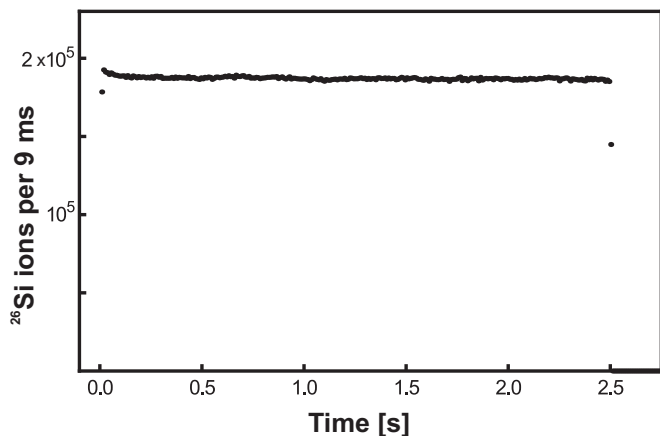


FIG. 3: Typical time-profile of the collected  $^{26}\text{Si}$  beam. The initial drop in intensity is generated by the change in gas density as the primary beam heats the gas around its path. A fan located inside the gas-target ensures a rapid transition to stable conditions.

No  $^{26}\text{Al}$  ions were present in the  $^{26}\text{Si}$  sample collected in our tape (see Sec. III C). Thus, if the sample collection rate were exactly constant, we could determine  $N_2/N_1$  from a simple calculation of the production of  $^{26}\text{Al}^m$  (via  $^{26}\text{Si}$  decay) over the precisely known time of the collection period. However, we measured the actual number of  $^{26}\text{Si}$  ions as a function of time with the scintillator at the exit of MARS and determined that there was a slightly higher rate at the very beginning of the collection period (see Fig. 3). Our cryo-target was a gas, and the primary beam heats that gas around its path through the target, thus initially generating a local drop in gas density; the transition to steady conditions was hastened by a fan that continuously circulated the gas in the target cell. We also found that the size of the variation in the radioactive-beam intensity at the beginning of a cycle depended on the primary beam intensity, potentially changing the beam-profile from one cycle to another. Nevertheless, with the collection time-profile measured and recorded for each cycle, we could perform a numerical integration over the measured  $^{26}\text{Si}$  accumulation to calculate the decay-production of  $^{26}\text{Al}^m$  and the corresponding  $N_2/N_1$  ratio accurately for each run.

### B. Parent-daughter relative efficiencies

The ratio  $\epsilon_1/\epsilon_2$  can also be established independently. In our experiment, we detected positrons from the decays of both  $^{26}\text{Si}$  and  $^{26}\text{Al}^m$  with a very low threshold and nearly 100% overall efficiency, so superficially one might conclude that  $\epsilon_1/\epsilon_2 = 1$  and that the efficiency ratio can consequently be ignored. However, the end-point energy of the  $\beta^+$  spectrum corresponding to the  $^{26}\text{Si}$  superallowed transition is 3819 keV, while that for the equivalent transition from  $^{26}\text{Al}^m$  is 3211 keV. The 608-keV difference between them means that the shapes

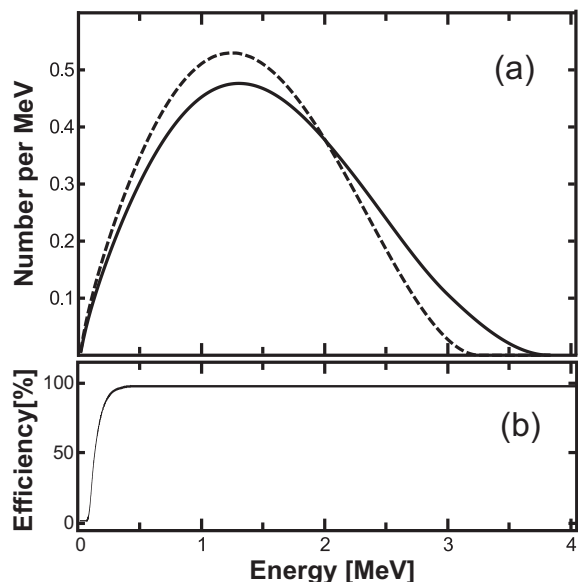


FIG. 4: (a) Calculated  $\beta^+$  spectra for  $^{26}\text{Si}$  (solid curve) and  $^{26}\text{Al}^m$  (dashed curve). The former includes the Gamow-Teller branches to  $1^+$  states as well as the superallowed branch to the  $0^+$  isomer; the latter is pure superallowed decay (see Fig. 1 for both decay schemes). (b) System efficiency for detecting positrons due to the effects of the aluminized Mylar tape and the Havar windows of the detector gas cells. The curve is the result of a Monte Carlo calculation.

of the two spectra are slightly different from one another. Furthermore, the Gamow-Teller branches that occur only for the  $^{26}\text{Si}$  decay contribute to the differences as well. This is illustrated by the calculated  $\beta^+$  spectra shown in Fig. 4(a).

Because we operate our gas detector in the plateau region (see Sec. II B), we can be confident that our electronic detection threshold is too low for losses from that source to have any effect on our overall detection efficiencies. However, the aluminized Mylar tape (half-thickness, 38  $\mu\text{m}$ ) and the Havar window of each detector gas cell (1.5  $\mu\text{m}$  thick) stop the lowest-energy positrons, thus preventing them from reaching the active volume of the detector. In effect, this imposes a low-energy cut-off and, since the parent and daughter  $\beta$  spectra have slightly different shapes at low energies, the fraction of positrons lost in one case is slightly different from that in the other. For a pair of decays like ours, where the average positron energy is greater for the parent than it is for the daughter, the ratio is always  $\epsilon_1/\epsilon_2 \geq 1$ .

Since the decay positrons are emitted isotropically, their paths through the tape and window cover a range of lengths, resulting in a low-energy cut-off that is not sharp. Nevertheless, for any given cut-off energy the effect on the efficiency ratio can readily be calculated from the known  $\beta$ -spectrum shapes. Using the Monte Carlo code EGSnrc (version V4-r2-3-0) [13], in which we modeled our exact tape/window/detector geometry, we obtained the overall system efficiency as a function of

positron energy, the result being shown in Fig. 4(b). Note that the code was only required to calculate the losses due to the tape and window. We have extensively tested [14] the accuracy of three Monte Carlo codes – EGSnrc, Geant4 and PENELOPE – in fitting experimental results from a thin scintillation detector for low energy conversion electrons as well as  $\beta$ -decay spectra. We found that EGSnrc offers the best combination: it agrees well with experiment and it operates most efficiently.

The Monte Carlo result was then integrated with each of the two spectra in Fig. 4(a) to obtain our overall efficiencies for detecting the parent and the daughter activities. From these, we derived the efficiency ratio,  $\epsilon_1/\epsilon_2 = 1.00143(25)$ , where we have assigned an uncertainty that encompasses a  $\pm 10\%$  relative uncertainty in the calculated ranges. This uncertainty was based on an assessment of how much the ratio would change if the source were not located at exactly the center of the detector, thus slightly changing the losses in the tape and window. However, by eliminating all cycles in which the ratio of recorded positrons to implanted silicon ions was anomalously low, we ensured that all analyzed cycles corresponded to central or nearly central source locations. The uncertainty we have assigned to the efficiency ratio is a very generous allowance for the range of locations allowed in the accepted cycles. The value we obtained for  $\epsilon_1/\epsilon_2$  and its uncertainty were subsequently used in the analysis of all runs.

### C. Sample impurities

From the position-sensitive detectors that we inserted into the MARS focal plane before the measurement and periodically during it, we could identify and monitor any reaction products that might potentially contribute as impurities to our selected  $^{26}\text{Si}$  beam. Only three were detectable and all were extremely weak:  $^{25}\text{Al}$  (0.02% of the  $^{26}\text{Si}$  intensity),  $^{24}\text{Al}$  (0.14%) and  $^{23}\text{Mg}$  (0.02%). However, even these small percentages must be reduced when we consider what was actually retained in the aluminized Mylar tape that transported the collected activity to our detector. As the impurity ions passed through our aluminum degraders, each impurity experienced a different energy loss from the others and from  $^{26}\text{Si}$ . The result is illustrated in Fig. 5 for the two thicknesses of degraders employed during the measurement (see Sec. II).

Figure 5 presents the results of calculations based on the SRIM code [15]. Before the main measurements began, we recorded the collected  $^{26}\text{Si}$  activity as a function of aluminum degrader thickness and were thus able to determine experimentally the precise thickness required to center the  $^{26}\text{Si}$  deposit in the tape. The value obtained was very close to that predicted by SRIM, which gives confidence that the calculations can be relied on to determine the spatial distributions of the impurities relative to that of  $^{26}\text{Si}$ . From Fig. 5 it is evident that only 10% of the  $^{24}\text{Al}$  and 50% of the  $^{23}\text{Mg}$  was collected in

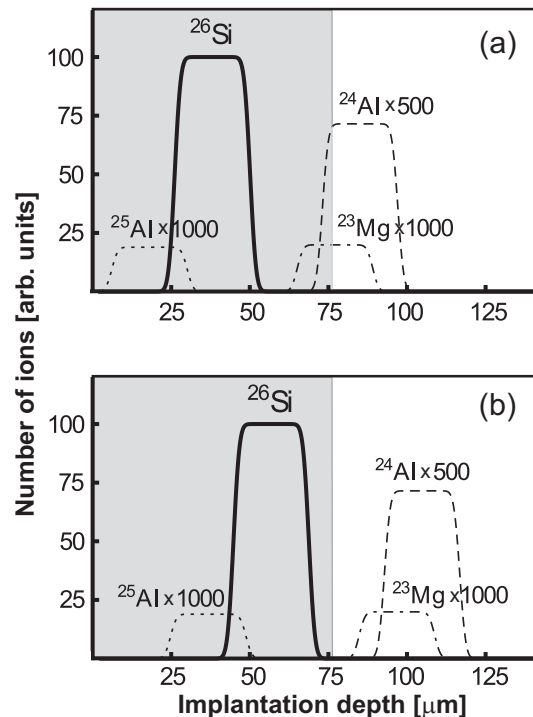


FIG. 5: Illustrations of calculated implantation profiles in Mylar for the  $^{26}\text{Si}$  beam and those impurities with similar ranges. All beams enter from the left. The top illustration (a) gives the profile after the beams have passed through 159  $\mu\text{m}$  of aluminum, while the bottom one (b) gives the result after 171  $\mu\text{m}$  of aluminum. The shaded region in both illustrations corresponds to the actual thickness of our collection tape. Those ions within the shaded region are collected in our sample; all others are not.

the tape when the  $^{26}\text{Si}$  was centered in the tape (top illustration) and none at all when the  $^{26}\text{Si}$  was placed near the back of the tape (bottom). Consequently, relative to the collected  $^{26}\text{Si}$  activity, the collected  $^{24}\text{Al}$  and  $^{23}\text{Mg}$  activities were both approximately 0.01% when the  $^{26}\text{Si}$  was centered; they were zero when it was near the back. The only remaining impurity,  $^{25}\text{Al}$ , was fully collected at both degrader settings, but its relative intensity was only 0.02% to start with. The effect of these three impurities was only barely significant, but we included them with their appropriate relative intensities when we fitted the collected decay spectra. We also incorporated a  $\pm 30\%$  relative uncertainty on the intensities used.

### D. Time decay analysis

We fitted the data from each of the 55 runs separately, incorporating four components:  $^{26}\text{Si}$ ; its daughter,  $^{26}\text{Al}^m$ ; the weak impurities,  $^{25}\text{Al}$ ,  $^{24}\text{Al}$  and  $^{23}\text{Mg}$ ; and a constant background. The half-life of  $^{26}\text{Al}^m$  was fixed at its known value of 6345.0(19) ms [1]. Its initial activity relative to that of  $^{26}\text{Si}$  was set for each run to the value obtained from numerical integration of the



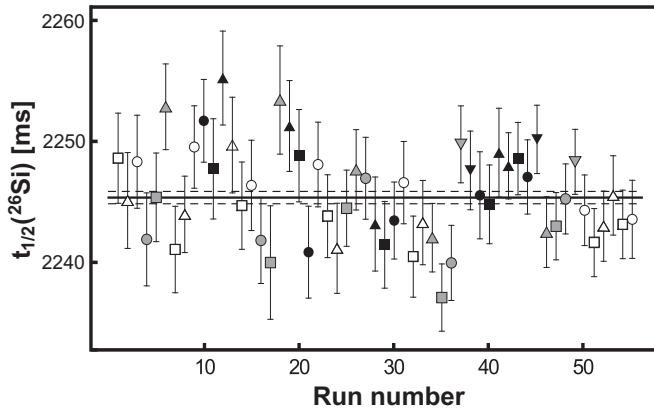


FIG. 6: Test for possible systematic bias in the  $^{26}\text{Si}$  half-life measurement due to discriminator threshold or detector voltage. Open/grey/black symbols represent the three discriminator settings, 150 mV/200 mV/250 mV; the four detector biases, 2550 V, 2650 V, 2750 V and 2850 V are represented by the symbol shapes  $\triangle$ ,  $\square$ ,  $\circ$  and  $\nabla$ , respectively. The average value for the half-life is 2245.26(51) ms (statistical uncertainty only) with  $\chi^2/\text{ndf} = 70.6/54$ . The average value appears as the solid line, with dashed lines as uncertainty limits.

measured time-profile for the collected  $^{26}\text{Si}$  beam in that run (see Sec. III A and Fig. 3); and the efficiency ratio,  $\epsilon_1/\epsilon_2$ , was fixed at the value established in Sec. III B. The half-lives of  $^{25}\text{Al}$ ,  $^{24}\text{Al}$  and  $^{23}\text{Mg}$  were taken to be 7.182(12) s [16], 2.053(4) s [6] and 11.324(10) s [16] respectively. Their initial relative activities were obtained from the measurement and calculations described in Sec. III C.

Since each run was obtained with a different combination of detection settings, we could use the individually fitted  $^{26}\text{Si}$  half-lives to test for any systematic dependence on those settings. As seen in Fig. 6, the half-life results show no systematic dependence on detector bias or discriminator threshold. Although not illustrated, the results were also found to be independent of both the imposed circuit dead time and the length of time for which the sample was collected. As a final systematic check, in this case for the possible presence of short-lived impurities or other possible count-rate dependent effects, we removed data from the first 0.9 s of the counting period in each measurement and refitted the remainder; then we repeated the procedure, removing the first 1.8 s, 2.7 s and so on. From Fig. 7 it can be seen that, within statistics, the derived half-life was also stable against these changes.

With these possible systematic effects eliminated as significant factors, we can combine all 55 runs to obtain a value for the  $^{26}\text{Si}$  half-life of  $t_{1/2}(^{26}\text{Si}) = 2245.26$  ms, with a statistical uncertainty of  $\pm 0.51$  ms. The normalized  $\chi^2$  of this average is 1.31 and the statistical uncertainty has been multiplied by the square root of this number. The result itself represents a self-consistent analysis of about 200 million combined  $^{26}\text{Si}$  and  $^{26}\text{Al}^m$  decay events.

This analysis has depended upon the source being centrally located in the gas counter for each cycle since serious misplacement would have resulted in a differ-

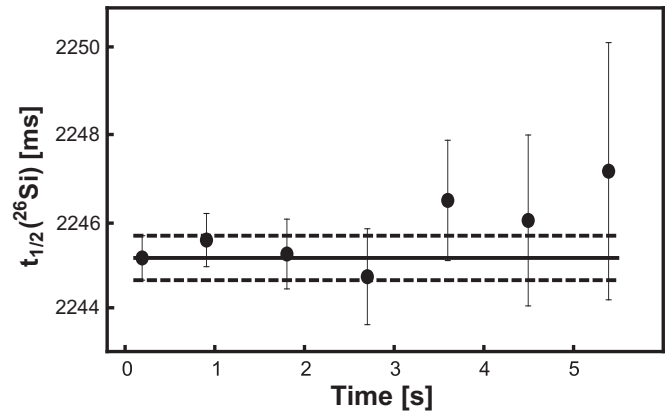


FIG. 7: Test for possible systematic bias in the  $^{26}\text{Si}$  half-life measurement caused by undetected short-lived impurities or by rate-dependent counting losses. Each point is the result of a separate fit to the data; the abscissa for each point represents the time period at the beginning of the counting cycle for which the data were omitted from that particular fit. The solid and dashed lines correspond to the average half-life value and uncertainties given in Fig. 6.

ent parent-daughter relative efficiency for that cycle (see Sec. III B). We ensured centrality by rejecting cycles that had anomalously low ratios of recorded positrons to implanted silicon ions. For each run we included only those cycles with ratios between 91 and 100% of the maximum value obtained for that run. To test whether our result is in any way sensitive to this choice, we repeated the full analysis for subgroups of the cycles corresponding to ratios between 98-100%, 96-98%, 94-96% and so on. Although having larger uncertainties, the half-lives obtained from those subgroups within our selected band of 91-100% were all statistically consistent with our quoted result of 2245.3(5) ms. More importantly, the nearest group of rejected cycles – those with ratios in the range 88-90% – were also consistent, yielding a value of 2246.7(30) ms. Clearly, our selection criterion for accepting cycles was a conservative one that does not adversely affect the result.

It is also interesting to compare this result with the half-life value derived from a fit to the data that does not impose a fixed link between the parent and daughter activities. We described in Secs. III A and III B how we could reduce by one the number of free parameters in the fit by independently determining the ratios  $N_2/N_1$  and  $\epsilon_1/\epsilon_2$ . This improved the statistical uncertainty in the fitted result but did introduce an additional uncertainty associated with the ratio  $\epsilon_1/\epsilon_2$  (see the second line in Table I). If we ignore the parent-daughter link and fit the data with four variable parameters (including background), we obtain a half-life result of 2243.2(22) ms, which is statistically consistent with the value presented in Table I but has a thrice larger uncertainty.

### E. Uncertainty budget

There are other contributions, of course, to our final uncertainty beyond the contribution from counting statistics. We itemize them all in Table I. Counting statistics is the largest contributor to the overall uncertainty, but the contribution associated with the different efficiencies for detecting parent and daughter activities is a close second. Less important contributors were the uncertainties in the  $^{26}\text{Al}^m$  half-life, the dominant circuit dead-time and the weak sample impurities. Our final result for the  $^{26}\text{Si}$  half-life is 2245.3(7) ms, in which statistical and systematic uncertainties have been combined.

### F. Comparison with previous results

Three previous measurements of the  $^{26}\text{Si}$  half-life are listed in the most recent review [1]: 2210(21) ms [17], 2240(10) ms [18] and 2228.3(27) ms [4]. The first two of these results were recorded more than 30 years ago and have uncertainties larger by more than a factor of 10 than our present result; one of them agrees with our result, while the other lies one-and-a-half of its standard deviations away. This can hardly be viewed as a matter of concern. However, the last of the previous measurements was published only two years ago, has a quoted uncertainty that is only four times ours and differs from our result by more than six times that uncertainty. This discrepancy has to be addressed.

In their measurement, Matea *et al.* [4] employed a purified  $^{26}\text{Si}$  beam from the JYFLTRAP Penning-trap facility and implanted it in a movable 100- $\mu\text{m}$ -thick Mylar tape located at the center of a hollow cylinder whose 2-mm-thick walls were made from plastic scintillator optically coupled to two photomultipliers. After sample implantation, the decay positrons were counted in the plastic scintillator, after which the tape removed the sample and the cycle was repeated. The experimental arrangement is pictured in Ref. [19]; there it can be seen that the tape enters and exits the scintillator cylinder via the same opening and passes over a roller, which is located within the cylinder.

The method Matea *et al.* used to analyze their data

was similar to ours in that they fixed the activity of  $^{26}\text{Al}^m$  based on its calculated production from the decay of an initially pure  $^{26}\text{Si}$  sample. Unfortunately they did not take account of any detection-efficiency difference between the parent and daughter activities [20] (see Sec. III B). Furthermore, their experimental conditions make this a much more serious problem for them than it was for us. First, both their thicker tape and the roller they used to allow that tape to move introduced a more significant and complicated low-energy cut-off due to positrons ranging out in those materials. Second, with a plastic scintillator and photomultiplier tubes generating their signals, they certainly needed to set a non-negligible low-energy electronic threshold. Third, their scintillator was, to some extent, sensitive to  $\gamma$  rays, which would slightly favor detection of  $^{26}\text{Si}$ , which produces  $\beta$ -delayed  $\gamma$  rays, while  $^{26}\text{Al}^m$  does not.

Although it is obviously impossible for us to model in detail someone else's experimental apparatus, we approximated their arrangement in the EGSnrc Monte Carlo code [13], the same code we used to help determine the efficiency ratio for our measurement (see Sec. III B). We found that the results were very sensitive to just those experimental details that we could not define precisely. Nevertheless, we determined that the value of  $\epsilon_1/\epsilon_2$  could easily reach 1.005 or possibly larger. If this ratio had been applied to their data, it would have increased their measured half-life by  $\sim 0.4\%$ , bringing it to 2237 ms, approximately half way to our result, and undoubtedly with a much larger uncertainty than the 2.7 ms originally claimed. Clearly this is only an indicative not a definitive calculation, since the exact correction and its application to the data requires information only available to the original authors. For now, though, we believe that it reveals a serious omission in the original analysis by Matea *et al.* [4], and that their published result should simply be discounted.

## IV. CONCLUSIONS

We report here the first measurement of the half-life of the superallowed  $\beta^+$  emitter  $^{26}\text{Si}$  obtained with a precision of better than 0.1%. Since  $^{26}\text{Si}$  and its daughter  $^{26}\text{Al}^m$  have comparable half-lives, this measurement required us to use the technique we developed for the measurement of the  $^{34}\text{Ar}$  half-life [5], in which we link the parent and daughter decays based on a precise knowledge of the rate of deposition of the  $^{26}\text{Si}$  source. We also had to make small but important corrections for detection-efficiency differences between the parent and daughter  $\beta^+$  decays. Possible sources of error were carefully investigated and an error budget established.

Our new precise result for the  $^{26}\text{Si}$  half-life, 2245.3(7) ms, is considerably different from the average value quoted in the most recent survey of world data for superallowed  $0^+ \rightarrow 0^+$   $\beta$ -decay transitions [1]. However, the average there is dominated by a measurement [4] that

TABLE I: Error budget for the  $^{26}\text{Si}$  half-life measurement.

Source	Uncertainty (ms)
statistics	0.51
efficiency ratio, $\epsilon_1/\epsilon_2$	0.37
$t_{1/2}(^{26}\text{Al}^m)$	0.16
dead time	0.07
sample impurities	0.04
Total	0.66
$^{26}\text{Si}$ half-life result (ms)	2245.3(7)



we now argue is flawed and should be discarded, since it leaves out the correction for parent-daughter detection-efficiency differences.

With our half-life result for  $^{26}\text{Si}$  decay having 0.03% precision, and the  $Q_{EC}$  value for its superallowed branch being recently determined to 0.0025% [3], the  $\mathcal{F}t$  value for the branch can in principle be determined to sub-0.1% precision if the branching ratio can be measured to that level. This is a difficult but potentially achievable goal and, if accomplished, would bring  $^{26}\text{Si}$  decay into the same category of precision as the best known superallowed transitions.

This would allow a particularly interesting comparison with its mirror,  $^{26}\text{Al}^m$  decay. If calculated with Saxon-Woods radial wave functions [2], the nuclear-structure-dependent correction,  $(\delta_C - \delta_{NS})$ , for the  $^{26}\text{Al}^m$  decay is 0.305(27)% [1], the smallest value for any superallowed transition, while the equivalent correction term for the

$^{26}\text{Si}$  decay is 0.650(34)%. The difference between them, 0.345(43)%, is reduced considerably, to 0.145(81)%, if Hartree-Fock wave functions are used instead [1]. An experimental determination of the difference between these mirror transitions with sub-0.1% precision would discriminate between these theoretical approaches and could potentially reduce the theoretical uncertainties that affect the ultimate determination of  $V_{ud}$  and the unitarity of the CKM matrix.

### Acknowledgments

This work was supported by the U.S. Department of Energy under Grant No. DE-FG03-93ER40773 and by the Robert A. Welch Foundation under Grant no. A-1397.

- 
- [1] J.C. Hardy and I.S. Towner, Phys. Rev. C **79**, 055502 (2009).
  - [2] I.S. Towner and J.C. Hardy, Phys. Rev. C **77**, 025501 (2008).
  - [3] T. Eronen, V.-V. Elomaa, U. Hager, J. Hakala, A. Jokinen, A. Kankainen, T. Kessler, I.D. Moore, S. Rahaman, J. Rissanen, C. Weber and J. Aysto, Phys. Rev. C **79**, 032802(R) (2009).
  - [4] I. Matea, J. Souin, J. Aysto, B. Blank, P. Delahaye, V.-V. Elomaa, T. Eronen, J. Giovinazzo, U. Hager, J. Hakala, J. Huikari, A. Jokinen, A. Kankainen, I.D. Moore, J.-L. Pedroza, S. Rahaman, J. Rissanen, J. Ronkainen, A. Saastamoinen, T. Sonoda and C. Weber, Eur. Phys. J. A **37**, 151 (2008).
  - [5] V.E. Iacob, J.C. Hardy, J.F. Brinkley, C.A. Gagliardi, V.E. Mayes, N. Nica, M. Sanchez-Vega, G. Tabacaru, L. Trache and R.E. Tribble, Phys. Rev. C **74**, 055502 (2006).
  - [6] P.M. Endt, Nucl. Phys. **A521**, 1 (1990).
  - [7] R.E. Tribble, A. Azhari, C.A. Gagliardi, J.C. Hardy, A. Mukhamedzhanov, X. Tang, L. Trache and S.J. Yennello, Nucl. Phys. **A701**, 278 (2002).
  - [8] V.T. Koslowsky, E. Hagberg, J.C. Hardy, R.E. Azuma, E.T.H. Clifford, H.C. Evans, H. Schmeing, U.J. Schrewe and K.S. Sharma, Nucl. Phys. **A405**, 29 (1983).
  - [9] V.T. Koslowsky, E. Hagberg, J.C. Hardy, G. Savard, H. Schmeing, K.S. Sharma and X.J. Sun, Nucl. Instrum. and Meth. in Phys. Res. A **401**, 289 (1997).
  - [10] J.C. Hardy, V.E. Iacob, M. Sanchez-Vega, R.G. Neilson, A. Azhari, C.A. Gagliardi, V.E. Mayes, X. Tang, L. Trache and R.E. Tribble, Phys. Rev. Lett. **91**, 082501 (2003).
  - [11] J.C. Hardy, V.E. Iacob, V. Golovko, J. Goodwin, N. Nica, H.I. Park, L. Trache and R.E. Tribble, Phys. Rev. C **77**, 045501 (2008).
  - [12] A handbook of radioactivity measurements procedures, National Council on Radiation Protection and Measurements report NCRP No 68, subsect. 2.2 (1985).
  - [13] I. Kawrakow, Med. Phys. **27**, 485 (2000); I. Kawrakow and D.W.O. Rogers, NRCC Report PIRS-701, NRC, Ottawa (2003); <http://www.irs.inms.nrc.ca/EGSsrc/EGSsrc.html>.
  - [14] V.V. Golovko, V.E. Iacob and J.C. Hardy, Nucl. Instr. and Meth. in Phys. Res. A **594**, 266 (2008); and to be published.
  - [15] J.F. Ziegler, <http://www.srim.org/#SRIM> (2008).
  - [16] N. Severijns, M. Tandecki, T. Phalet and I.S. Towner, Phys. Rev. C **78**, 055501 (2008).
  - [17] J.C. Hardy, H. Schmeing, J.S. Geiger and R.L. Graham, Nucl. Phys. **A246**, 61 (1975).
  - [18] H.S. Wilson, R.W. Kavanagh and F.M. Mann, Phys. Rev. C **22**, 1696 (1980).
  - [19] A. Bey, B. Blank, G. Canchel, C. Dossat, J. Giovinazzo, I. Matea, V.-V. Elomaa, T. Eronen, U. Hager, J. Hakala, A. Jokinen, A. Kankainen, I.D. Moore, H. Penttila, S. Rinta-Antila, A. Saastamoinen, T. Sonoda, J. Aysto, N. Adimi, G. de France, J.-C. Thomas, G. Voltolini and T. Chaventre, Eur. Phys. J. A **36**, 121 (2008).
  - [20] B. Blank, private communication (2008).